

A Posteriori Error Estimates for a Discontinuous Galerkin Method Applied to Elliptic Problems Log number: R74

Béatrice Rivière and Mary F. Wheeler

The Center for Subsurface Modeling, TICAM, The University of Texas, Austin
TX 78712, USA

Abstract. *A posteriori* error estimates for locally mass conservative methods for subsurface flow are presented. These methods are based on discontinuous approximation spaces and referred as Discontinuous Galerkin methods. In the case where penalty terms are added to the bilinear form, one obtains the Non-symmetric Interior Penalty Galerkin methods. In a previous work, we proved optimal rates of convergence of the methods applied to elliptic problems. Here, h adaptivity is investigated for flow problems in 2D. We derive global explicit estimators of the error in the L^2 norm and we numerically investigate an implicit indicator of the error in the energy norm. Model problems with discontinuous coefficients are considered.

1 Introduction

Finite element methods for elliptic problems based on discontinuous approximation spaces have been studied since the early seventies by Wheeler [12], Percell and Wheeler [10], Arnold [2,3]. Penalty terms enforced locally the continuity of the computed solution. Only recently, Baumann and Oden [5] introduced a new Discontinuous Galerkin (DG) method for the solution of pure diffusion problem. The convergence of the DG method was proven by Oden, Babuška and Baumann [8] in 1D, and by Rivière, Wheeler and Girault [11] in 2D and 3D. The addition of penalty terms to the DG scheme yields another discontinuous finite element method, namely the Non-symmetric Interior Penalty Galerkin (NIPG) method, introduced and analyzed in [11].

Recent years have seen the development of the theory of error estimation for Galerkin methods. The idea is to derive estimates of the error that only depend on the computed solution. Once obtained, these estimates can be used as a mean of controlling adaptively the computational process. A variety of *a posteriori error* estimates has been developed and analyzed. In a non-exhaustive list, one can refer to the work of Babuška et al [4], Ainsworth and Oden [1], Oden and Prudhomme [9] for some of the techniques applied to the continuous finite element method.

The goal of this paper is to investigate error estimation for the DG and NIPG methods. After introducing the schemes in the following section, we derive

and prove *a posteriori* error estimates in the L^2 norm in Section 3. Section 4 contains the definition and the numerical investigation of error indicators in the H^1 norm. Finally, the last section contains some concluding remarks.

2 Statement of the Problem. Finite Element Methods

2.1 Notation and Approximation Properties

Let Ω be a polygonal domain in \mathbb{R}^n , $n = 2, 3$. Let $\mathcal{E}_h = \{E_1, E_2, \dots, E_{N_h}\}$ be a non-degenerate subdivision of Ω , where E_j is a triangle or a quadrilateral if $n = 2$, or a tetrahedron, a prismatic or hexaedral element if $n = 3$. Let h_j be the diameter of E_j and let $h = \max\{h_j, j = 1 \dots N_h\}$. We denote the edges (resp. faces for $n = 3$) of \mathcal{E}_h by $\{e_1, e_2, \dots, e_{P_h}, e_{P_h+1}, \dots, e_{M_h}\}$ where e_k has positive $n - 1$ dimensional Lebesgue measure, $e_k \subset \Omega$ for $1 \leq k \leq P_h$, and $e_k \subset \partial\Omega$ for $P_h + 1 \leq k \leq M_h$. With each edge (or face) e_k , we associate a unit vector ν_k normal to e_k . For $k > P_h$, ν_k is taken to be the unit outward vector normal to $\partial\Omega$. For $s \geq 0$, let

$$H^s(\mathcal{E}_h) \equiv \{v \in L^2(\Omega) : v|_{E_j} \in H^s(E_j), j = 1 \dots N_h\}.$$

We now define the average and the jump for $\phi \in H^s(\mathcal{E}_h)$, $s > \frac{1}{2}$. Let $1 \leq k \leq P_h$; for $e_k = \partial E_1^k \cap \partial E_2^k$ with ν_k exterior to E_1^k , set

$$\{\phi\} = \frac{1}{2}(\phi|_{E_1^k})|_{e_k} + \frac{1}{2}(\phi|_{E_2^k})|_{e_k}, \quad [\phi] = (\phi|_{E_1^k})|_{e_k} - (\phi|_{E_2^k})|_{e_k}.$$

We consider a symmetric positive definite matrix-valued function $K = (k_{ij})_{1 \leq i, j \leq n}$, $K \in L^\infty(\Omega)$ and a nonnegative scalar function $\alpha \in L^\infty(\Omega)$. The usual Sobolev norm of H^m on $E \subset \mathbb{R}^n$ is denoted by $\|\cdot\|_{m,E}$. We define the following ‘‘broken’’ norms for m positive integer:

$$\|\Phi\|_m \equiv \left(\sum_{j=1}^{N_h} \|\Phi\|_{m,E_j}^2 \right)^{\frac{1}{2}}.$$

Let r be a positive integer. The finite element subspace is taken to be

$$\mathcal{D}_r(\mathcal{E}_h) \equiv \{v \in L^2(\Omega) : v|_{E_j} \in P_r(E_j) \quad \forall j = 1, \dots, N_h\},$$

where $P_r(E_j)$ denotes the set of polynomials of degree less than or equal to r on E_j .

We recall the following *hp* approximation properties, proven in [6,7], for $n = 2$. We will assume that these results also hold in the case $n = 3$. Let $E \in \mathcal{E}_h$ and $\phi \in H^s(E)$. Then there exists a constant C depending on s but independent of ϕ, r and h and a sequence $z_r^h \in P_r(E_j)$, $r = 1, 2, \dots$ such that for any

$$0 \leq q \leq s$$

$$\|\phi - z_r^h\|_{q,E} \leq C \frac{h_E^{\mu-q}}{r^{s-q}} \|\phi\|_{s,E}, \quad s \geq 0, \quad (1)$$

$$\|\phi - z_r^h\|_{\delta,e} \leq C \frac{h_E^{\mu-\frac{1}{2}-\delta}}{r^{s-\frac{1}{2}-\delta}} \|\phi\|_{s,E}, \quad s > \left(\frac{1}{2} + \delta\right), \quad \delta = 0, 1, \quad (2)$$

where $\mu = \min(r + 1, s)$, $h_E = \text{diam}(E)$ and $e \subset \partial E$.

2.2 Problem and Non-symmetric Bilinear Form

Let the boundary of the domain $\partial\Omega$ be the union of two disjoint sets Γ_D and Γ_N . We denote $\boldsymbol{\nu}_D$ (respectively $\boldsymbol{\nu}_N$) the unit normal vector to each edge of Γ_D (respectively Γ_N) exterior to Ω . For f given in $L^2(\Omega)$, p_0 given in $H^{\frac{1}{2}}(\Gamma_D)$ and g given in $L^2(\Gamma_N)$, we consider the following elliptic problem:

$$\boxed{\begin{aligned} -\nabla \cdot (K \nabla p) + \alpha p &= f && \text{in } \Omega, \\ p &= p_0 && \text{on } \Gamma_D, \\ K \nabla p \cdot \boldsymbol{\nu}_N &= g && \text{on } \Gamma_N. \end{aligned}} \quad (3)$$

With the assumptions on K and α stated in the previous section, problem (3) has a unique solution in $H^1(\Omega) \cap H^2(\mathcal{E}_h)$ when $|\Gamma_D| > 0$ or when $\alpha \neq 0$. For K in $W^{1,4}(\mathcal{E}_h)$ and $\psi, \phi \in H^2(\mathcal{E}_h)$, we consider the non-symmetric bilinear form:

$$\begin{aligned} a_{NS}(\psi, \phi) &= \sum_{j=1}^{N_h} \int_{E_j} (K \nabla \psi \nabla \phi + \alpha \psi \phi) \\ &\quad - \sum_{k=1}^{P_h} \int_{e_k} \{K \nabla \psi \cdot \boldsymbol{\nu}_k\} [\phi] + \sum_{k=1}^{P_h} \int_{e_k} \{K \nabla \phi \cdot \boldsymbol{\nu}_k\} [\psi] \\ &\quad - \int_{\Gamma_D} (K \nabla \psi \cdot \boldsymbol{\nu}_D) \phi + \int_{\Gamma_D} (K \nabla \phi \cdot \boldsymbol{\nu}_D) \psi. \end{aligned}$$

We define the linear form:

$$L(\phi) = (f, \phi) + \int_{\Gamma_D} (K \nabla \phi \cdot \boldsymbol{\nu}_D) p_0 + \int_{\Gamma_N} \phi g.$$

2.3 Finite Element Schemes

The Discontinuous Galerkin approximation P^{DG} in $\mathcal{D}_r(\mathcal{E}_h)$ satisfies the formulation

$$\boxed{a_{NS}(P^{\text{DG}}, v) = L(v), \quad \forall v \in \mathcal{D}_r(\mathcal{E}_h).} \quad (4)$$

The addition of penalty terms to the DG scheme yields another discontinuous Galerkin method. These penalty terms are defined as follows

$$J_0^{\sigma,\beta}(\phi, \psi) = \sum_{k=1}^{P_h} \frac{\sigma_k}{|e_k|^\beta} \int_{e_k} [\phi][\psi] + \sum_{e_k \in \Gamma_D} \frac{\sigma_k}{|e_k|^\beta} \int_{e_k} \phi \psi,$$

where σ is a discrete positive function that takes the constant value σ_k on the edge or face e_k , $|e_k|$ denotes the measure of e_k and $\beta \geq \frac{1}{2}$ is a real number. The Galerkin approximation P^{NIPG} in $\mathcal{D}_r(\mathcal{E}_h)$ solves the following discrete problem:

$$a_{NS}(P^{\text{NIPG}}, v) + J_0^{\sigma,\beta}(P^{\text{NIPG}}, v) = L(v) + \sum_{e_k \in \Gamma_D} \frac{\sigma_k}{|e_k|^\beta} \int_{e_k} p_0 v, \quad \forall v \in \mathcal{D}_r(\mathcal{E}_h). \quad (5)$$

We refer to [8,11] about the consistency of the two schemes and the existence and uniqueness of the discrete solutions.

2.4 Residual and orthogonality equations

Here, we state two equations that are important in the analysis of the error estimators. Let $e^{\text{DG}} = p - P^{\text{DG}}$ (resp. $e^{\text{NIPG}} = p - P^{\text{NIPG}}$) be the error in the DG method (resp. the NIPG method). Then, the following residual equations are satisfied for any v in $H^2(\mathcal{E}_h)$

$$a_{NS}(e^{\text{DG}}, v) = L(v) - a_{NS}(P^{\text{DG}}, v),$$

$$\begin{aligned} a_{NS}(e^{\text{NIPG}}, v) + J_0^{\sigma,\beta}(e^{\text{NIPG}}, v) &= L(v) - a_{NS}(P^{\text{NIPG}}, v) \\ &\quad + \sum_{e_k \in \Gamma_D} \frac{\sigma_k}{|e_k|^\beta} \int_{e_k} p_0 v - J_0^{\sigma,\beta}(P^{\text{NIPG}}, v), \end{aligned}$$

and the following orthogonality equations are satisfied for any v in $\mathcal{D}_r(\mathcal{E}_h)$

$$\begin{aligned} a_{NS}(e^{\text{DG}}, v) &= 0, \\ a_{NS}(e^{\text{NIPG}}, v) + J_0^{\sigma,\beta}(e^{\text{NIPG}}, v) &= 0. \end{aligned}$$

3 A Posteriori Error Estimation in the L^2 norm

We first define residual quantities that only depend on the approximate solution and the data. The residuals consist of interior residuals and boundary residuals described below

$$R_{\text{int}}|_E = f + \nabla \cdot (K \nabla P^{\text{DG}}) - \alpha P^{\text{DG}}, \quad \forall E \in \mathcal{E}_h,$$

$$R_b^1 = [K \nabla P^{\text{DG}} \cdot \boldsymbol{\nu}_k] \quad 1 \leq k \leq P_h, \quad R_b^1 = g - K \nabla P^{\text{DG}} \cdot \boldsymbol{\nu}_N \quad \text{on } \Gamma_N,$$

$$R_b^2 = [P^{\text{DG}}] \quad 1 \leq k \leq P_h, \quad R_b^2 = p_0 - P^{\text{DG}} \quad \text{on } \Gamma_D.$$

We assume that Ω is convex, $\Gamma_N = \partial\Omega$ and K is sufficiently smooth so that the solution ϕ of the dual problem

$$\begin{aligned} -\nabla \cdot (K\nabla\phi) + \alpha\phi &= e^{\text{DG}}, \quad \text{in } \Omega, \\ \phi &= 0, \quad \text{on } \partial\Omega, \end{aligned}$$

belongs to $H^2(\Omega)$, with continuous dependence on e^{DG} .

Theorem 1. L^2 *a posteriori* error estimate for the DG method

$$\|e^{\text{DG}}\|_{0,\Omega} \leq C \left(\sum_{j=1}^{N_h} \eta_{0,j,\text{DG}}^2 \right)^{\frac{1}{2}}$$

where

$$\begin{aligned} \eta_{0,j,\text{DG}}^2 &= \frac{h_j^4}{r^4} \|R_{\text{int}}\|_{0,E_j}^2 + \sum_{e_k \subset \partial E_j \cap \partial\Omega} \frac{h_j^3}{r^3} \|R_b^1\|_{0,e_k}^2 \\ &+ \sum_{e_k \subset \partial E_j \setminus \partial\Omega} \left(\frac{\hat{h}_{e_k}^3}{2r^3} \|R_b^1\|_{0,e_k}^2 + \frac{\hat{h}_{e_k}}{2r} \|R_b^2\|_{0,e_k}^2 + \frac{1}{\hat{h}_{e_k}} \|R_b^2\|_{0,e_k}^2 \right) \end{aligned}$$

where $\hat{h}_{e_k} = \max(h_i, h_j)$ for $e_k = \partial E_i \cap \partial E_j$ and C is a constant that is independent of h and r .

Proof. To simplify the writing, we will use the notation e for the error e^{DG} . Then,

$$\|e\|_{0,\Omega}^2 = \sum_{j=1}^{N_h} \int_{E_j} (-\nabla \cdot (K\nabla\phi) + \alpha\phi)e.$$

Integrating by parts on each element and using the fact that the jumps $[K\nabla\phi \cdot \boldsymbol{\nu}_k]_{e_k} = 0$, we obtain

$$\|e\|_{0,\Omega}^2 = \sum_{j=1}^{N_h} \int_{E_j} (K\nabla\phi\nabla e + \alpha\phi e) - \sum_{k=1}^{P_h} \int_{e_k} \{K\nabla\phi \cdot \boldsymbol{\nu}_k\}[e],$$

Let ϕ^* be a continuous approximation of ϕ satisfying the properties (1)-(2). By subtracting the orthogonality equation $a_{NS}(e, \phi^*) = 0$, we obtain

$$\begin{aligned} \|e\|_{0,\Omega}^2 &= \sum_{j=1}^{N_h} \int_{E_j} (K\nabla(\phi - \phi^*)\nabla e + \alpha(\phi - \phi^*)e) \\ &+ \sum_{k=1}^{P_h} \int_{e_k} \{K\nabla(\phi - \phi^*) \cdot \boldsymbol{\nu}_k\}[e] - 2 \sum_{k=1}^{P_h} \int_{e_k} \{K\nabla\phi \cdot \boldsymbol{\nu}_k\}[e]. \quad (6) \end{aligned}$$

We integrate by parts the first term of the right-hand side of Equation (6)

$$\begin{aligned}
\|e\|_{0,\Omega}^2 &= \sum_{j=1}^{N_h} \int_{E_j} R_{\text{int}}(\phi - \phi^*) + \sum_{k=1}^{P_h} \int_{e_k} (\phi - \phi^*) R_b^1 + \int_{\partial\Omega} R_b^1(\phi - \phi^*) \\
&\quad + \sum_{k=1}^{P_h} \int_{e_k} \{K \nabla(\phi - \phi^*) \cdot \boldsymbol{\nu}_k\} R_b^2 - 2 \sum_{k=1}^{P_h} \int_{e_k} \{K \nabla \phi \cdot \boldsymbol{\nu}_k\} R_b^2 \\
\|e\|_{0,\Omega}^2 &\leq \sum_{j=1}^{N_h} \|R_{\text{int}}\|_{0,E_j} \|\phi - \phi^*\|_{0,E_j} \\
&\quad + \sum_{k=1}^{P_h} \|\{\phi - \phi^*\}\|_{0,e_k} \|R_b^1\|_{0,e_k} + \sum_{e_k \subset \partial\Omega} \|R_b^1\|_{0,e_k} \|\phi - \phi^*\|_{0,e_k} \\
&\quad + \sum_{k=1}^{P_h} \|K\|_{\infty} \|\{\nabla(\phi - \phi^*) \cdot \boldsymbol{\nu}_k\}\|_{0,e_k} \|R_b^2\|_{0,e_k} \\
&\quad + 2 \sum_{k=1}^{P_h} \|K\|_{\infty} \|\{\nabla \phi \cdot \boldsymbol{\nu}_k\}\|_{0,e_k} \|R_b^2\|_{0,e_k}
\end{aligned}$$

If we denote by \hat{h}_{e_k} the minimum of the diameters of the elements that share the common edge (or face) e_k , and if we apply the approximation results (1)-(2), we deduce

$$\begin{aligned}
\|e\|_{0,\Omega}^2 &\leq C \|\phi\|_{2,\Omega} \left(\sum_{j=1}^{N_h} \frac{h_j^4}{r^4} \|R_{\text{int}}\|_{0,E_j}^2 \right. \\
&\quad + \sum_{k=1}^{P_h} \frac{\hat{h}_{e_k}^3}{r^3} \|R_b^1\|_{0,e_k}^2 + \sum_{e_k \subset \partial\Omega} \frac{\hat{h}_{e_k}^3}{r^3} \|R_b^1\|_{0,e_k}^2 \\
&\quad \left. + \sum_{k=1}^{P_h} \|K\|_{\infty}^2 \frac{\hat{h}_{e_k}}{r} \|R_b^2\|_{0,e_k}^2 + 2 \sum_{k=1}^{P_h} \frac{\|K\|_{\infty}^2}{\hat{h}_{e_k}} \|R_b^2\|_{0,e_k}^2 \right)^{\frac{1}{2}}
\end{aligned}$$

The theorem is then obtained by using the regularity of the adjoint problem. \square

The same technique applies to the NIPG method and an easy modification of the proof stated above enables us to prove the following error estimate.

Theorem 2. *L^2 a posteriori error estimate for the NIPG method*

$$\|e^{\text{NIPG}}\|_{0,\Omega} \leq C \left(\sum_{j=1}^{N_h} \eta_{0,j,\text{NIPG}}^2 \right)^{\frac{1}{2}}$$

where

$$\begin{aligned} \eta_{0,j,\text{NIPG}}^2 &= \frac{h_j^4}{r^4} \|R_{int}\|_{0,E_j}^2 + \sum_{e_k \subset \partial E_j \cap \partial \Omega} \frac{h_j^3}{r^3} \|R_b^1\|_{0,e_k}^2 + \sum_{e_k \subset \partial E_j \setminus \partial \Omega} \frac{1}{\hat{h}_{e_k}} \|R_b^2\|_{0,e_k}^2 \\ &+ \sum_{e_k \subset \partial E_j \setminus \partial \Omega} \frac{1}{2} \left(\frac{\hat{h}_{e_k}^3}{r^3} \|R_b^1\|_{0,e_k}^2 + \frac{\hat{h}_{e_k}}{r} \|R_b^2\|_{0,e_k}^2 + \frac{\sigma_k^2 \hat{h}_{e_k}^4}{|e_k|^{2\beta} r^4} \|R_b^2\|_{0,e_k}^2 \right) \end{aligned}$$

where $\hat{h}_{e_k} = \max(h_i, h_j)$ for $e_k = \partial E_i \cap \partial E_j$ and C is a constant that is independent of h and r .

Even though these theoretical estimates are important for the analysis of the DG and NIPG methods, in practice, they cannot be used to estimate the error since they involve unknown constants. The rest of this paper will deal with the construction of robust error indicators for which there are no unknown constants.

4 Numerical Study of Mesh Adaptation

The purpose of this section is to first define error indicators in the energy norm that are implicitly computed on each element of the mesh. Then, these error indicators are tested on several problems. We first define a linear functional R and bilinear forms b_j

$$\begin{aligned} R(v) &= L(v) - a_{NS}(P^{DG}, v), \quad \forall v \in H^2(\mathcal{E}_h), \\ b_j(\Phi, v) &= \int_{E_j} (K \nabla \Phi \nabla v + \alpha \Phi v) - \int_{\partial E_j} (K \nabla \Phi \cdot \nu_{E_j}) v \\ &+ \int_{\partial E_j} (K \nabla v \cdot \nu_{E_j}) \Phi, \quad \forall \Phi, v \in H^2(\mathcal{E}_h), \quad 1 \leq j \leq N_h \end{aligned}$$

and we introduce the local discrete problem: find Φ_h in $\mathcal{D}_{r+q}(\mathcal{E}_h)$ such that

$$b_j(\Phi_h, v) = R(v), \quad \forall v \in \mathcal{D}_{r+q}(E_j), \quad 1 \leq j \leq N_h,$$

where q is a positive integer. We note that $\mathcal{D}_{r+q}(\mathcal{E}_h)$ is a larger (richer) space than $\mathcal{D}_r(\mathcal{E}_h)$ and we will refer to q as the degree of enrichment of the space. The error indicator for the energy norm of e^{DG} is denoted by η_1 and defined by

$$\eta_1 = \left(\sum_{j=1}^{N_h} \eta_{1,j}^2 \right)^{\frac{1}{2}}, \quad \eta_{1,j}^2 = b_j(\Phi_h, \Phi_h). \quad (7)$$

In all our numerical experiments, we locally refine the elements E_j which exhibit large error indicators $\eta_{1,j}$. Therefore, an element E_{j_0} is refined if $\eta_{1,j_0} / \max_j \eta_{1,j} \geq \delta$ where δ is a parameter ranging between 0 and 1. We

will fix $\delta = 0.50$ in all the following numerical experiments. The quality of the error estimator is measured by the effectivity index γ defined as: $\gamma = \eta_1 / (a_{NS}(e, e))^{1/2}$. We now study the robustness the error indicator η_1 for several test problems.

4.1 The Bubble Function

In this first example, the elliptic problem (3) is solved on the unit square $(0, 1)^2$ with the data chosen such that the exact solution is the bubble function $p(x, y) = x(x - 1)y(y - 1)$. Dirichlet boundary conditions are applied. The tensor K is the identity tensor and we consider the two cases: $\alpha = 0$ and $\alpha = 1$.

We first study the influence of the degree of the enriched space on the performance of the global error indicator η_1 , for a given finite element mesh. The degree of the enriched space ($r + q$) is varied between 3 and 10, with r fixed at 2. The behavior of the effectivity index γ is shown in Fig. 1 (a) for various fixed meshes of size h_m , $0 \leq m \leq 4$, where $h_m = 2^{-(m+1)}$. It is seen that, as expected, the effectivity index converges to unity as q is increased. Note that the effectivity index is approximately 0.9, even when the mesh is coarse (denoted by h_0 , with just 4 elements).

Next, we fix the degree of the enriched space at 7 and study the behavior of γ as the mesh is refined using the adaptation strategy described in Section 4. The resulting behavior is shown in Fig. 2 (a). The effectivity index stays close to unity as the mesh is subdivided and no significant oscillations are observed.

The experiments described in the preceding paragraphs are repeated with $\alpha = 1$, and the corresponding results are shown in Fig. 1 (b) and Fig. 2 (b). The behavior of the effectivity index γ is virtually unchanged. This suggests that the indicators η_1 is not very sensitive to the presence of the lower order term in the governing partial differential equation.

4.2 The “Peak” Function

Our goal here is to study the performance of the error indicator η_1 and the effectiveness of the adaptation strategy presented in Section 4, when the solution has high gradients. For this purpose, we consider a solution that satisfies problem (3) on the unit square, represented in Fig. 3. The exact solution is given by $p(x, y) = 0.0005x^2(x - 1)^2y^2(y - 1)^2e^{10x^2+10y}$. It is not a symmetric function and it contains a “peak” that indicates a great variation in the gradient. The tensor K is the identity tensor and we consider two cases: $\alpha = 0$ and $\alpha = 1$. We will see that the results obtained in both cases are quantitatively and qualitatively similar. The degree of the DG approximation takes the values 2, 3 and 4. As before, the effectivity indices are investigated on a sequence of uniform meshes for different degrees of enrichment.

From Fig. 4 ($r = 2$), Fig. 5 ($r = 3$), and Fig. 6 ($r = 4$), we see that, for a given mesh, the effectivity index converges to unity as the degree of the enriched space is increased. The indicator underestimates the error when the mesh is coarse and the degree of enrichment is low. However, as the degree of DG approximation is increased, we observe an improvement in the behavior of the effectivity index.

We now investigate the performance of the adaptation strategy. We adaptively subdivide the mesh with $\delta = 0.50$, using the strategy presented earlier. We begin with a uniform mesh of size $h = 1/2$. The variation of the effectivity index γ is shown in Fig. 7 for different values of r and q . We see that, as r the degree of approximation is increased, the effectivity index moves closer to unity.

Next, we study the behavior of the true error in the H^1 seminorm with respect to the adaptation strategy, in Fig. 8. In this figure, the relative error, defined as $(a_{NS}(e^{DG}, e^{DG})/a_{NS}(p_{ex}, p_{ex}))^{1/2}$ is plotted against the number of degrees of freedom. We fix $q = 5$, and vary r between 2 and 4. For each r , we consider the cases of uniform and adaptive subdivisions. We see that the adaptive strategy using error indicator η_1 consistently outperforms the uniform subdivision strategy and enables the recovery of the optimal rate of convergence.

In Fig. 9, we show the final meshes and solutions resulting from the adaptive subdivision strategy for the cases $r = 2$ and $r = 4$. We see that the error indicator accurately predicts regions of high gradients, thus leading to meshes that are appropriately subdivided.

4.3 Problem with Discontinuous Coefficients

The purpose of this section is to investigate the behavior of the DG method and the effect of the implicit error indicator η_1 described earlier for solutions of problem (3) with discontinuous coefficients. The domain $\Omega = (-1, 1)^2$ is divided in four sub-domains Ω_i as shown in Fig.10. The tensor K takes the constant value K_i over each sub-domain and we assume that $K_1 = K_3$ and $K_2 = K_4$. We seek an analytical solution of the form $r^\alpha(a_i \sin(\alpha\theta) + b_i \cos(\alpha\theta))$, where (r, θ) are the polar coordinates of a given point in Ω and a_i, b_i are constants that depend on the sub-domains Ω_i . The analytical solution p_{ex} satisfies the usual interface conditions, namely the continuity of the solution and the normal fluxes across the interfaces. It is known that p_{ex} belongs to the Sobolev space $H^{1+\alpha}(\Omega)$. Dirichlet boundary conditions are assumed. We consider two cases: $(K_1, K_2) = (100, 1)$ and $(K_1, K_2) = (5, 1)$.

Case: $(K_1, K_2) = (100, 1)$:

In that case, the solution presents a singularity around the origin and we can show that the parameters characterizing the analytical solution are $\alpha = 0.1269, a_1 = 0.100, b_1 = 1.000, a_2 = -9.604, b_2 = 2.960, a_3 = -0.480, b_3 = -0.883, a_4 = 7.701, b_4 = -6.456$.

We first analyze the convergence of the DG solution on a sequence of uniformly subdivided meshes. The coarse mesh consists of the four sub-domains Ω_i . The relative error in the L^2 norm, defined as $\|e^{\text{DG}}\|_0/\|p\|_0$ is plotted against the number of degrees of freedom in Fig. 11. The degree of the polynomial approximation varies between 2 and 5. We see, as expected, that the convergence rate does not depend on the degree of the approximation, but that it depends on the regularity of the solution. In that case, the numerical convergence rate in the L^2 norm is $O(h^{2\alpha}) = O(h^{0.25})$, where h is the mesh size, or $O(N^{-\alpha})$, where N is the number of degrees of freedom. Due to numerical integration errors arising around the origin, one has to compute the H^1 seminorm of the exact solution by using the Green's theorem and by computing a line integral over $\partial\Omega$.

In Fig. 12 (a), the convergence of the quantity $A^* = a_{NS}(P^{\text{DG}}, P^{\text{DG}}) - a_{NS}(p_{ex}, p_{ex})$ is studied for a degree of polynomial approximation between 2 and 5. It is observed that the rate of convergence is $O(h^{2\alpha})$ or $O(N^{-\alpha})$, which is the optimal rate usually obtained in the conforming finite element method. As above, the rate of convergence does not depend on the degree r of polynomial approximation. We now investigate the robustness of the adaptation strategy. We begin with a uniform mesh of size $h = 1$ and we adaptively subdivide the mesh with $\delta = 0.50$ using the strategy described above. We fix $r = 2$ and $q = 5$ and we show in Fig. 13 (a) the final mesh and solution. We see that the mesh is appropriately subdivided around the origin.

Figure 13 (b) shows the error indicators computed on each element. The error indicators are larger in the neighborhood of the origin, which means that the implicit error indicator capture very well the location of the singularity of the exact solution. Fig. 14 (a) and 14 (b) show a close-up view of the computed solution and the local error indicators at the origin. Here, we see that the error indicators possess the same symmetry properties than the exact solution. In Fig. 15 (a), the mesh adaptation strategy yields an optimal convergence rate that is not obtained in the case of uniform mesh subdivisions.

Case $(K_1, K_2) = (5, 1)$:

In that case, the exact solution is smoother than above, and we can show that the parameters characterizing the solution are $\alpha = 0.5354, a_1 = 0.4472, b_1 = 1.000, a_2 = -0.7453, b_2 = 2.333, a_3 = -0.9441, b_3 = 0.5556, a_4 = -2.402, b_4 = -0.4815$.

We repeat the experiments described above with $K_1 = 5$. In particular, the convergence rates of the error in the L^2 norm and of the quantity A^* defined above are considered in Fig. 11 (b) and Fig. 12 (b) for quadratic and cubic DG solutions. As expected, the convergence rate for both quantities is $O(h^{2\alpha}) = O(N^{-\alpha})$ and does not depend on the degree r of polynomial approximation. Since α is greater than 0.5, numerical integration does not pollute the computation of the energy norm and we see in Fig. 15 (b) that the convergence rate of the error in the energy norm is $O(h^\alpha) = O(N^{-\alpha/2})$, as

expected. Here again, adaptive mesh refinements lead to optimal convergence rates.

We conclude the study of mesh adaptation for this example, by investigating the efficiency of the error indicator. For that, we consider the final mesh obtained with the adaptive subdivision strategy for $q = 5$. Given a box of size H centered around the origin, we count the number of elements that are contained in the box. Figure 16 shows the plots for the two cases studied above. One observes that the indicator efficiently captures the singularity of the exact solution around the origin since 72% of the elements are contained in the box of size $H = 0.1$, which corresponds to a subdomain of size $1/400$ of the size of the domain. In the case where $K_1 = 5$, i.e., the exact solution is less singular than in the case of $K_1 = 100$, and 44% of the elements are contained in the box of size $H = 0.1$.

5 Conclusion

In this work, we have derived *a posteriori* estimates of the error in the L^2 norm for a class of methods based on discontinuous approximation spaces. We have also presented a new adaptive strategy to control the numerical error of the discontinuous Galerkin solutions. This strategy is based on the local computation of an implicit indicator of the error in the energy norm. In that case, the study shows the robustness and efficiency of the error indicator, even when the coefficients of the elliptic equation are discontinuous. Besides, the error indicator shows great potential if used as an error estimator.

6 Acknowledgments

The authors wish to thank Prof. Ivo Babuška and Dr. Serge Prudhomme for their valuable suggestions and constructive comments.

References

1. Ainsworth M., Oden J.T.: A posteriori error estimation in finite element analysis. TICAM Report 96-19 (1996)
2. Arnold D.N.: An interior penalty finite element method with discontinuous elements. Ph.D. Thesis. University of Chicago. (1979)
3. Arnold D.N.: An interior penalty finite element method with discontinuous elements. SIAM J. Numer. Anal. **19** (1982) 724–760
4. Babuška I., Zienkiewicz O.C., Gago J., Oliveira E.A.: Accuracy Estimates and Adaptive Refinements in Finite Element Computations. Wiley (1986)
5. Baumann C.E.: An h-p adaptive discontinuous finite element method for computational fluid dynamics. Ph.D. Thesis. The University of Texas at Austin. (1997)
6. Babuška I., Suri M.: The h-p version of the finite element method with quasiuniform meshes. Mathematical Modeling and Numerical Analysis **21-2** (1987)

7. Babuška I., Suri M.: The optimal convergence rate of the p-version of the finite element method. *SIAM J. Numer. Anal.* **24-4** (1987)
8. Oden J.T., Babuška I., Baumann C.E.: A discontinuous hp finite element method for diffusion problems. *J. Compu. Phys.* **146** (1998) 491–519
9. Oden J.T., Prudhomme S.: A technique for a posteriori error estimation of h-p approximations of the Stokes equations. *Adv. Adap. Comp. Meth. Mech.* **47** (1998) 43–63
10. Percell P., Wheeler M.F.: A local residual finite element procedure for elliptic equations. *SIAM J. Numer. Anal.* **15** (1978) 705–714
11. Rivière B., Wheeler M.F, V. Girault: Improved energy estimates for interior penalty, constrained and discontinuous Galerkin methods for elliptic problems. Part I. *Computational Geosciences* **3** (1999) 337–360
12. Wheeler M.F.: An elliptic collocation-finite element method with interior penalties. *SIAM J. Numer. Anal.* **15** (1978) 152–161

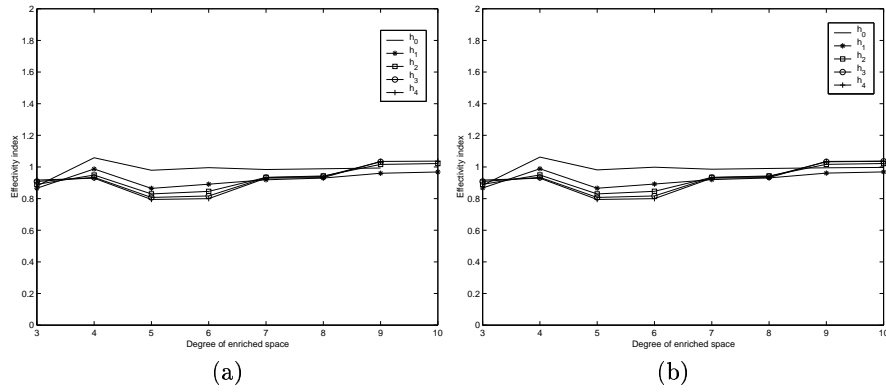


Fig. 1. Effectivity index v . the degree of enriched space for the bubble function. (a) $\alpha = 0$, (b) $\alpha = 1$.

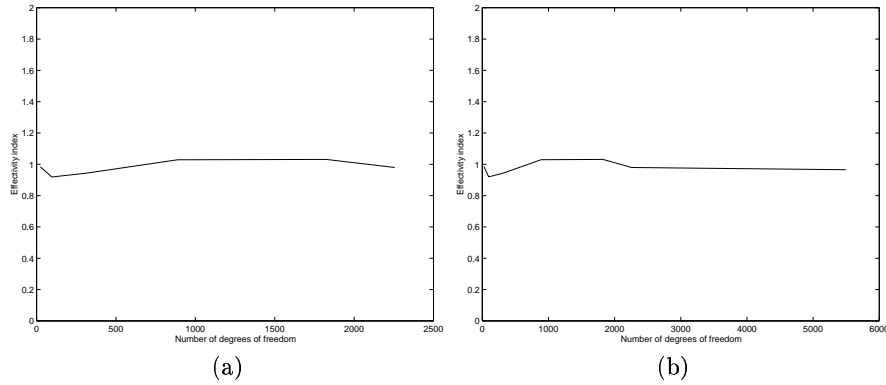


Fig. 2. Effectivity index v . the number of degrees of freedom for the bubble function. $r = 2$, $q = 5$. (a) $\alpha = 0$, (b) $\alpha = 1$.

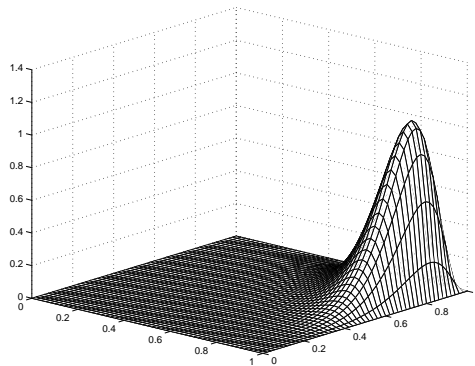


Fig. 3. Exact solution.

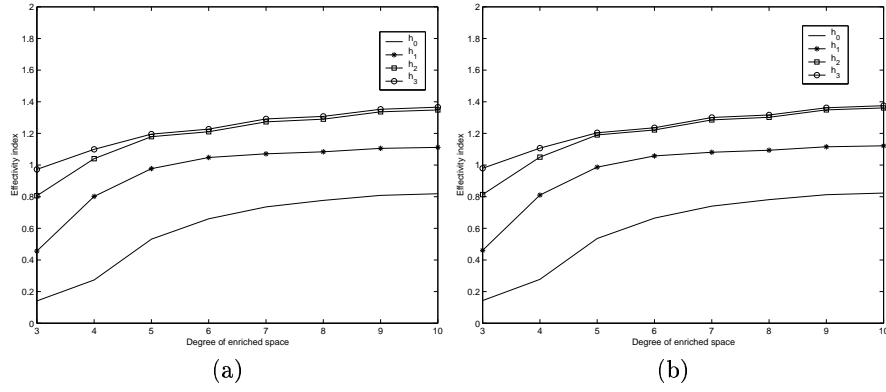


Fig. 4. Effectivity index v. the degree of enriched space for $r = 2$. (a) $\alpha = 0$, (b) $\alpha = 1$.

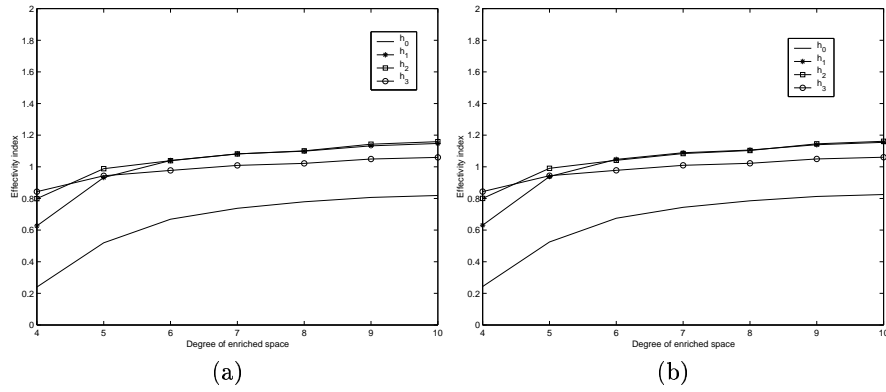


Fig. 5. Effectivity index v. the degree of enriched space for $r = 3$. (a) $\alpha = 0$, (b) $\alpha = 1$.

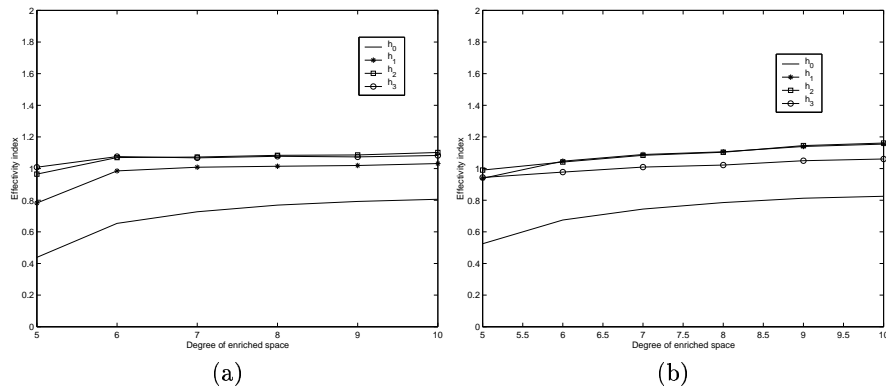


Fig. 6. Effectivity index v. the degree of enriched space for $r = 4$. (a) $\alpha = 0$, (b) $\alpha = 1$.

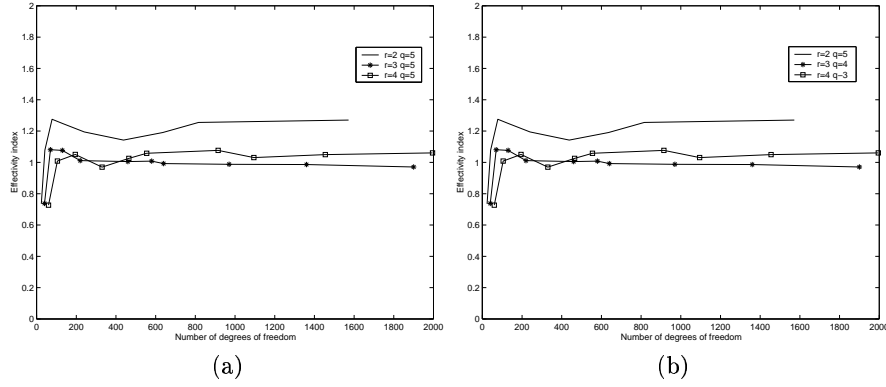


Fig. 7. Effectivity index ν , the number of degrees of freedom using an adaptive subdivision of the mesh. (a) $\alpha = 0$, (b) $\alpha = 1$.

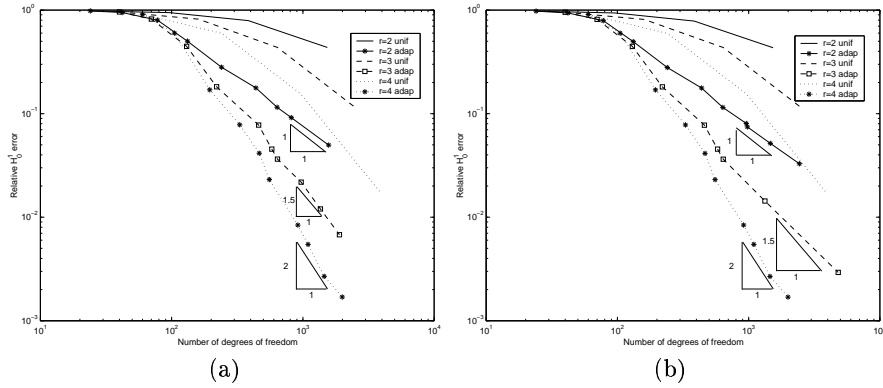


Fig. 8. Relative error in the energy norm ν , the number of degrees of freedom using an adaptive or uniform subdivision of the mesh. (a) $\alpha = 0$, (b) $\alpha = 1$.

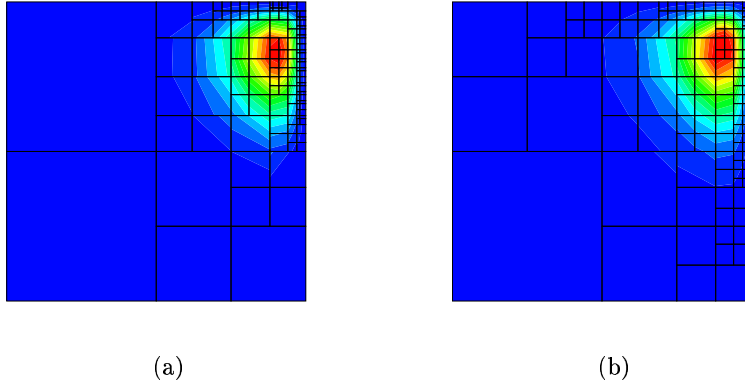


Fig. 9. Computed DG solution obtained on the adaptively subdivided mesh for $\alpha = 0$. (a) $r = 2$, (b) $r = 4$.

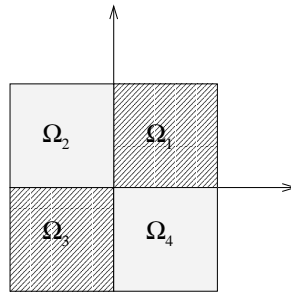


Fig. 10. Initial domain for the problem with discontinuous coefficients.

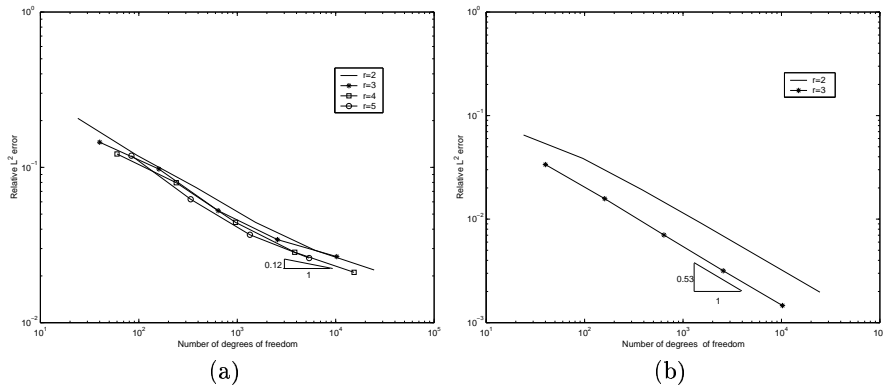


Fig. 11. Relative error in the L^2 norm v. the number of degrees of freedom for uniformly subdivided meshes. (a) $K_1 = 100$, (b) $K_1 = 5$.

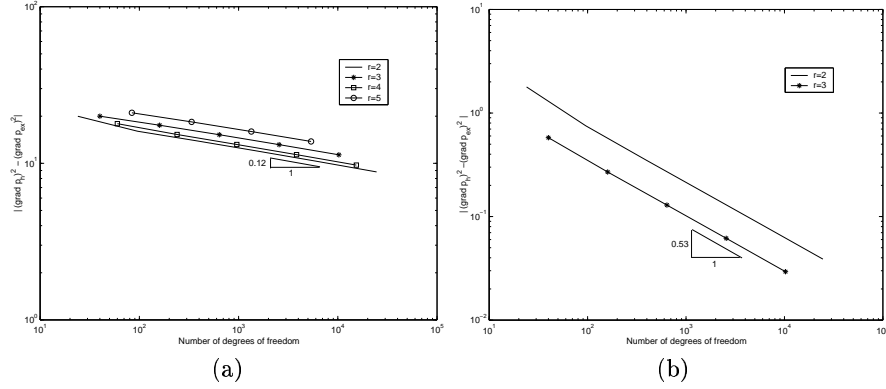


Fig. 12. Quantity A^* v. the number of degrees of freedom for uniformly subdivided meshes. (a) $K_1 = 100$, (b) $K_1 = 5$.

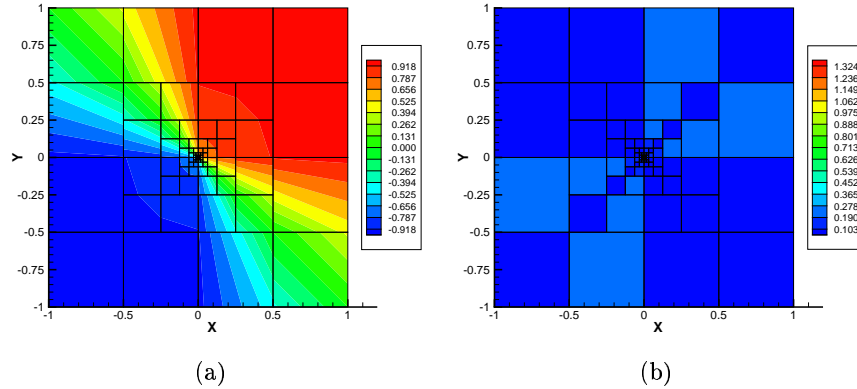


Fig. 13. (a) Computed solution on adaptive mesh, (b) Local error indicators on adaptive mesh. $r = 2$, $q = 5$, $K_1 = 100$.

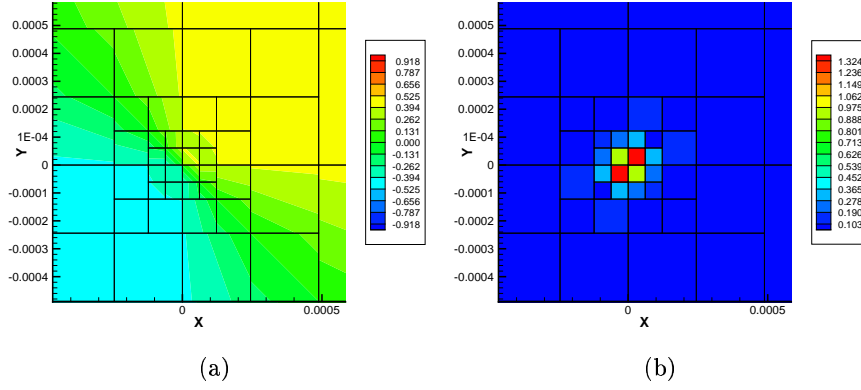


Fig. 14. (a) Close-up view of DG solution on adaptive mesh, (b) Close-up view of error indicators on adaptive mesh. $r = 2$, $q = 5$, $K_1 = 100$.

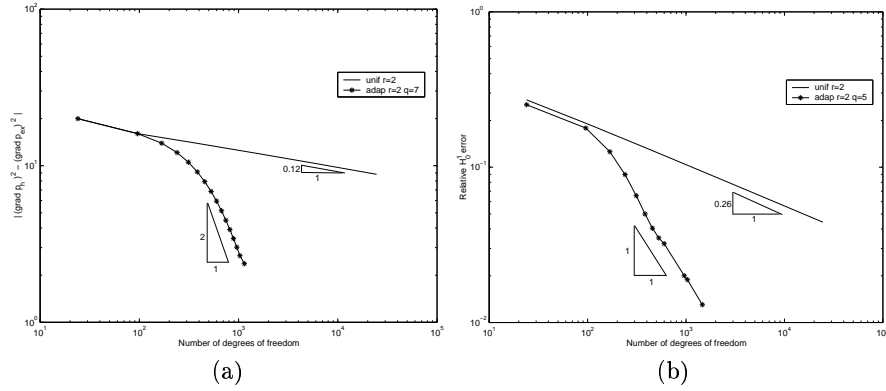


Fig. 15. (a) Quantity A^* v. the number of degrees of freedom for $K_1 = 100$, (b) Relative error in the energy norm v. the number of degrees of freedom for $K_1 = 5$. $r = 2$, $q = 5$.

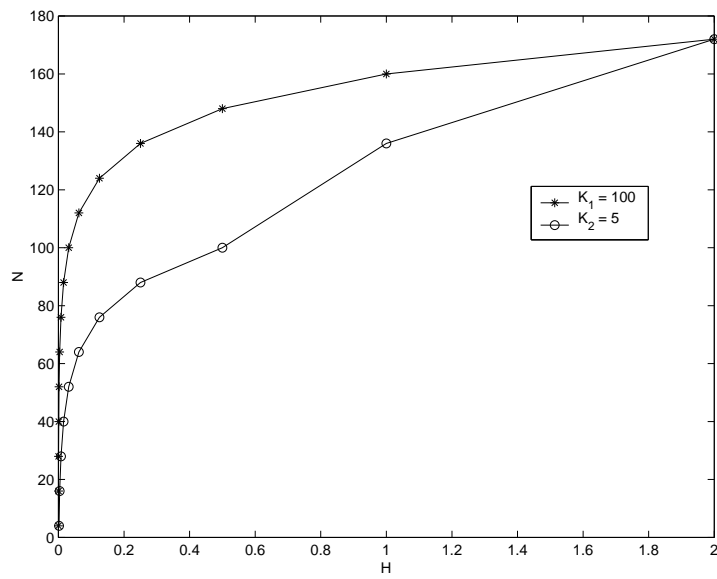


Fig. 16. Number of elements contained in a box of size H for $r = 2$, $K_1 = 100$ and $K_1 = 5$.